Applied Catalysis B: Environmental 244 (2019) 327–339

Contents lists available at ScienceDirect

Applied Catalysis B: Environmental

journal homepage: www.elsevier.com/locate/apcatb

Single-site Pt/La-Al_2O_3 stabilized by barium as an active and stable catalyst in purifying CO and C_3H_6 emissions

Hui Wang[a], Jinshi Dong[a], Lawrence F. Allard[c], Sungsik Lee[d], Se Oh[b], Jun Wang[a], Wei Li[b,*], Meiqing Shen[a,*], Ming Yang[b,*]

[a] School of Chemical Engineering & Technology, Tianjin University, Tianjin 300350, China
[b] Chemical and Materials Systems Laboratory, General Motors Global Research and Development, 30470 Harley Earl Blvd, Warren, MI 48092, USA
[c] Materials Science and Technology Division, Oak Ridge National Laboratory, Oak Ridge, TN 37831, USA
[d] X-ray Science Division, Argonne National Laboratory, Argonne, IL 60439, USA

ARTICLE INFO

Keywords:
Single-atom catalyst
Platinum
High-temperature stability
Emissions purification
Alumina

ABSTRACT

High-temperature operations present a substantial challenge for developing industrial-capable precious metal catalysts (e.g. Pt/alumina), where the scarce metal atoms easily become wasted as sintered nanoparticles. Using fully dispersed precious metal atoms to deliver the catalysis remains an elusive goal. On a widely used La-stabilized alumina support, we find that the atomically dispersed Pt_1(II)-O_x- species, rather than the much more visible large metal particles, are the actual catalytic sites for the CO and C_3H_6 oxidation reactions. Unfortunately, the La dopants in alumina support will not hinder the sintering of the active Pt_1(II)-O_x- species. As a natural next step, the Ba-O_x- species were introduced to specifically stabilize the single-atom Pt on the La-stabilized alumina support. By implementing this improved formulation, the atomically dispersed Pt on alumina retains the original full dispersion even after 650 °C hydrothermal aging. Intriguingly, with or without the barium additives and/or sintered platinum particles in the catalysts, the intrinsic activity per Pt atom stays intact. Along with other experimental evidence, this leads to the finding that the single-atom Pt is the true catalytic site for the oxidation of CO and C_3H_6 in the widely-used Pt/La-Al_2O_3 material system. This work provides a new perspective for efficient precious metal utilization under demanding catalytic conditions.

1. Introduction

Atomically dispersed supported metal catalysts may offer full catalytic efficiency in many reactions if the sintering of the dispersed atoms can be hindered [1,2]. Examples from the recent literature and our authors' work have explored ways to prepare such catalysts as stable dispersions that can withstand various reaction conditions from room temperature up to 400 °C [3–6]. However, the stability of these catalysts, especially on an earth-abundant oxide support like alumina-based materials, is limited to low temperatures, below 300 °C. Single-site isolated Pt, Au, and Pd, stabilized but not saturated in coordination by the surface oxygen linkages, are active for CO oxidation [7–9], NO oxidation [10], and the water-gas shift reaction [3–6,11]. It has been shown that using reducible cerium-based oxides as the catalyst support is an effective approach to improve the thermal stability of the dispersed metal atoms [11–13]. However, in addition to the limited elemental abundance of the cerium-based oxides, the use of these oxides may negatively affect the oxidation of HCs and NOx under an oxygen-rich atmosphere — the typical operating conditions for modern lean-burn gasoline and diesel engines [14,15]. The general issue of how to stabilize the catalytically active platinum metal single atoms on earth-abundant and low-cost substrates, such as the widely used La-stabilized alumina by industry, in various demanding reaction conditions remains largely unresolved.

It is critical to build these single-site platinum or other precious metal atoms so that they remain stable and active under severe reaction conditions. This is especially true for the automotive exhaust applications, where almost one half of the annual global platinum group metal (PGM) production is used in the engine emissions control catalysts. Currently, over 90% of PGM is wasted due to the sintering in a typical working catalyst. The issue of stable activity in demanding conditions is thus important both from a fundamental viewpoint, but also for robust catalyst designs in practical applications. The failures of dispersing the platinum metals on alumina-based materials and retaining these dispersions at automotive exhaust conditions have been known for decades. For example, highly active atomic Pd sites dispersed on the La-

* Corresponding authors.
E-mail addresses: wei.1.li@gm.com (W. Li), mqshen@tju.edu.cn (M. Shen), ming.yang@gm.com (M. Yang).

https://doi.org/10.1016/j.apcatb.2018.11.034
Received 21 August 2018; Received in revised form 1 November 2018; Accepted 14 November 2018
Available online 19 November 2018
0926-3373/

alumina supports sinter rapidly into large, discrete particles at temperatures as low as 100 °C [9]. On the other hand, Pt single atoms in alumina and silica can be fully coordinated and stabilized by various organic ligands and precursors up to 400 °C, but poor catalytic activities of these over-stabilized Pt atoms have been reported [16,17]. As a general case, it is documented that, upon heating up to a threshold temperature of 600 °C for a few minutes, the formation of large platinum particles from atomic migration resulted in a two to tenfold decline in metal dispersion [18–20]. A desired PGM-catalyst must survive high-temperature spikes and still deliver low-temperature activities. This principle hinders the application of the current single-atom PGM platforms to a variety of high-temperature catalytic processes, in particular the catalytic purification of vehicle exhaust where the temperature of the feed gas stream can easily exceed 600 °C.

A few elements regarded as chemical promoters have been studied as stabilizers to hinder the PGM sintering. The La additives have been widely used in vehicle emissions control catalysts. Lanthanum dopants significantly improve the thermal stability of the γ-Al_2O_3 by anchoring on the penta-coordinated Al^{3+} sites and thus inhibiting the alumina phase transition [21,22]. For the stability of the PGMs, Montimi et al. impregnated platinum with an average size of 1.4 nm on Al_2O_3 support with La_2O_3 dopants, and found the catalyst can maintain the glycerol conversion over a period of 50 h at 350 °C [23]. Araújo et al. showed that Pt nanoparticles ranging from 1 to 5 nm supported on 12 wt.% La_2O_3 doped Al_2O_3 kept stable after 24 h of the dry reforming of methane reaction at 600 °C [24]. Peterson et al. speculated that the addition of La can stabilize the single-atom Pd species through oxygen bond that was created after calcination at elevated temperatures [9]. However, these single-atom Pd species, as the most ideally dispersed active sites, went through a fast sintering under the CO oxidation reaction stream from as low as 100 °C. Similarly, we found in the present work that the single-site Pt on La-Al_2O_3 aggregated into large nanoparticles after a hydrothermal aging at 650 °C, despite the encouraging atomic dispersion of Pt in the as-prepared fresh catalysts. This again highlights the low stability of the finely dispersed PGM species that leads to the significant loss of the catalytic activity after extensive use. As for the low-temperature water-gas shift reaction that our authors worked on previously, it is possible to retain the atomic dispersions of the active PtO_x- species on alumina, silica, zeolites, and titania by stabilizing them with a shell of alkali ions though –O bonds. Extended operation at 275 °C for many hours is thus possible [6]. Still, these preparations would not withstand the high-temperature spikes of the automotive exhaust operation (See supporting information (SI) for the K-stabilized catalysts). The well-known issue of alkali metal loss in emission control catalysts after prolonged operation is another reason that we chose to find the alternatives to the alkali metal stabilizers [25]. Due to the similarities of group I and II elements in electronegativity (e.g. Na: 0.93; K: 0.82; Ba: 0.89.) that are critical for binding with the next metal atom through -O- linkages, the barium naturally emerges as a promising stabilizer for the dispersed Pt catalytic species. However, the optimal effectiveness and the nature of the mitigated catalysis has not been systematically explored. Herein, we first report a new group of active and stable Pt/La-Al_2O_3 catalysts using BaO additives with almost 100% atomic dispersion (0.4 wt.% Pt) after hydrothermal aging up to 650 °C, and examine their coordination and activity for the oxidation of CO and C_3H_6 at simulated lean-burn emission conditions.

2. Experimental

2.1. Catalyst preparation

The commercial La-Al_2O_3 support (5% La-stabilized γ-Al_2O_3, SOLVAY Rhodia) was used after calcination at 400 °C for 10 h in flowing air. To establish the [Pt]–[Group II metal] interaction through −O− linkages (to be proved in the following sections), it is crucial to have the −O− [Group II metal] species bridge easily to the Pt atom center during the catalyst preparation. The Pearson's Hard-Soft (Lewis) Acid-Base (HSAB) principle defines the Pt atom as the soft acid, which thermodynamically prefers binding to ligands having higher degrees of softness, such as the oxygen-based O^{2-}, −OH, and NO_3- ligands [26,27]. Therefore, the barium nitrate was adopted as the additive precursors in this work. Pertaining to the amount of barium additives, we use a trace amount of barium, aiming to generate a shell of -O-Ba binding layer around the Pt atom center to allow the latter to be adequately stabilized. Our corresponding author M. Yang and his coworkers had demonstrated that the ratio of 1:6 to 1:10 is the optimal for alkali metals with a combination of experiment and DFT calculations [3,6]. When it applied to the alkaline earth elements with larger atomic numbers and atom radius, we figured the 1:5 ratio is adequate to form the sinter-resistant shell as EXAFS fitting results have shown. From a practical point of view, the solubility of many barium precursors is not high in general, and 1:5 is a reasonable ratio to ensure the full generation of barium ions in aqueous environment during the synthesis. Higher loadings of Ba additives may well lead to catalyst pore blocking and the formation of $BaCO_3$ and other NO_x trap component that will not serve the purpose of stabilizing Pt cations. In short, we are trying to create the highly dispersed -O-Ba species on catalyst surface that can interact with the isolated Pt ions. These species will form exclusively only at low barium loadings [28], and we do not need abundant barium additives (e.g. 10–20 wt.%) to form the typical lean NO_x trap component such as carbonates to complicate material system with spectator/irrelevant components to the catalysis [29,30]. The barium-stabilized Pt-Ba/La-Al_2O_3 samples were prepared by sequential incipient wetness impregnations (IWI) of chloroplatinic acid and barium nitrate with an interval vacuum drying process at room temperature (RT) for 12 h. These impregnated powders were dried in vacuum at 70 °C overnight, and then transferred to a furnace to calcine in flowing air at 550 °C for 2 h (heating rate 1 °C/min) to obtain what we denote as "fresh" catalysts. The conventional baseline Pt/La-Al_2O_3 catalysts were prepared by IWI, using the same parameters but without adding alkaline earth additives. The actual loading for Pt determined by inductively coupled plasma atomic emission spectroscopy (ICP-AES) ranged from 0.4 to 1.5 wt.% depending on the sample design, and the weight percentage of platinum was labeled as the numbers at the front of each sample name. In this work, we chose to use a near 0.5 wt.% Pt loading for in-depth studies of atomically dispersed Pt, because we estimated from the metal dispersion of the ~1.5 wt.% Pt catalysts (Table 1) that the maximal capacity of the support to carry the fully dispersed Pt was about 0.5 wt.%. The minor difference of 0.4 vs 0.5 or 1.4 vs 1.5 wt.% for catalysts with and without Ba was due to the weight dilution from Ba. For per surface area of the support, the actual concentration of Pt on the La-Al_2O_3 support was designed to be the same during the sample preparation.

The 1.2Pt-Ce/La-Al_2O_3 catalyst was synthesized by the same approach as that for the Pt-Ba/La-Al_2O_3 catalysts. Cerium nitrate was the precursor (Pt:Ce atomic ratio = 1:10).

X-ray fluorescence (XRF) analysis confirmed the full removal of –Cl residuals after the calcination at 550 °C. The Pt-free materials comprising the barium additives were prepared by IWI onto La-Al_2O_3. Without platinum, these samples did not bring any noticeable catalytic behavior in either of the reactions (CO and C_3H_6 oxidation) nor probe

Table 1
The overall structural properties and Pt dispersions of the platinum catalysts.

Sample	Overall texture	Pt dispersion (%)†
0.5Pt/La-Al_2O_3 fresh	Average pore size	77
0.5Pt/La-Al_2O_3 aged	~10 nm;	24
0.4Pt-Ba/La-Al_2O_3 fresh	Adsorption isotherm IV	95
0.4Pt-Ba/La-Al_2O_3 aged	For all samples;	90
1.5Pt/La-Al_2O_3 aged	BET surface area:	17
1.4Pt-Ba/La-Al_2O_3 aged	190 ± 7 m^2/g_{cat}	36

molecule characterizations (CO chemisorption), as was the case for the bare alumina support. All the platinum catalysts were stored under ambient conditions (no need to block light or air to maintain catalyst stability) before any in situ treatments and tests.

The hydrothermally aged samples were obtained by treating the catalysts in flowing air with 10% steam at 650 °C for 2 h (ramping rate: 10 °C/min). In line with the earlier reports studying the sintering of the supported platinum species [18–20], we found the chosen aging temperature and atmosphere incurred rapid sintering of platinum in the baseline catalysts. We also excluded any noticeable loss of platinum loading due to the metal vaporization by using the above aging condition. An obvious Pt vaporization was observed after 750 °C hydrothermal aging for 2 h, which is a separate cause of catalyst deactivation [31,32]. The stable γ-Al_2O_3 is the common structure detected in all the samples, and the additives do not modify the overall structure of the support. In fact, to form compounds between alkaline earth metals and alumina, calcination to above 800 °C for many hours is required [33]. The control synthesis allows us to focus on the role of platinum chemistry in defining the catalytic performances.

2.2. Materials characterization

The BET surface area and porosity of the samples were measured by multiple-point N_2 adsorption and desorption cycles in a Micromeritics ASAP 2020 instrument. A typical physisorption analysis started with an evacuation stage that held at 90 °C for 60 min followed by a heating stage at 350 °C. Both of these stages were at the pressure of 100 mmHg.

The XRD analysis was performed on a D8 advance diffractometer. Cu Kα radiation (λ = 1.5418 Å) was used with a power setting of 50 kV and 250 mA. A scan rate of 2°/min with a 0.02° step size was used.

The number of the exposed platinum surface (Pt dispersion) was measured by CO chemisorption in a Micromeritics AutoChem 2920 instrument. In a typical measurement, a 100 mg sample was first treated with 10% O_2/He at 350 °C for 60 min, and was then treated with 10% H_2/Ar at 350 °C for 30 min. The catalyst was cooled down to 45 °C in a 50 mL/min He purge, and was stabilized under that condition for 30 min. The 10% CO/He pulses were injected into the sample tube to start the chemisorption measurement, and a TCD detector recorded the concentration signals. The CO-Pt adsorption ratio was assumed to be 1:1. However, possible bridge (CO:Pt = 1:2) and trifold (CO:Pt = 1:3) adsorption modes on nearby Pt atoms will reduce the actual dispersion value. Speaking of the legitimate use of the 1:1 ratio under CO chemisorption measurement conditions, there are a few classic papers showing that the 1:1 is a common ratio used for reliable cross comparison [34,35]. We conducted the CO DRIFTS experiment on the two representative aged samples under the same CO chemisorption conditions to probe the possible contributions from different CO adsorption modes. As shown in Fig. S3, the linear CO adsorption on Pt is obviously the dominated species on our key samples after aging, where the sintered Pt particles with extended metal surfaces prevalently exist on the aged baseline Pt/La-Al_2O_3 sample. Therefore, the use of CO: Pt adsorption ratio as 1:1 was appropriate in this study.

High-angle annular dark-field (HAADF) images of Pt single-atom dispersions on alumina were obtained at 200 kV using a JEOL 2200FS STEM/TEM instrument housed in the Advanced Microscopy Laboratory at Oak Ridge National Laboratory. The 2200FS is equipped with a CEOS GmbH (Heidelberg, Ger.) aberration corrector on the probe-forming lenses; the images were acquired at a collection semi-angle of 26.5 mr, with a nominal beam current of 30 pA, and with the HAADF detector having inner and outer collection angles of 110 and 470 mr, respectively. Typical images of single atoms were recorded at 10 Mx direct magnification, using 32 or 64 μs pixel dwell times to give scan times of 8.5 or 17 s, respectively. Because the nanoparticles and sub-nm species have almost equal chance to be imaged on the thin and flat support surfaces, the platinum species (> 300 total counts) near the edge of the support particles in different regions were counted and analyzed.

The X-ray absorption spectroscopy (XAS) scans were collected in a fluorescence mode with a 13-channel Ge detector at the 12-BM of the Advanced Photon Source (APS) at Argonne National Laboratory. The X-ray absorption edge energy for Pt L_{III} $2p_{3/2}$ edge was calibrated to 11,564 eV by Pt foil in each scan. For each data collection point, five consecutive scans (each lasts for about 30 min) were acquired. The reaction-spent catalyst had been stabilized in three cycles of light-off tests (H_2 pretreatment; Reaction: 5000 ppm CO- 500 ppm HCs- 1.0% O_2- 5% H_2O- N_2 balance; 100–350 °C; ramping rate: 2 °C/min) and cooled down to RT in N_2 purge. The reference spectra of Pt(IV), Pt(II), and Pt(0) (i.e. PtO_2, $Pt(NH_3)_4(NO_3)_2$, and Pt foil) were collected at RT in static air. The Feff models of Pt foil, PtO_2 film, PtO film, and Ba_4PtO_6 were used to fit the 1st shell Pt–Pt and Pt–O coordination conditions. The X-ray absorption near edge structure (XANES) data was processed by the Athena software, and the extended X-ray absorption fine structure (EXAFS) data was analyzed by the Artemis software.

The X-ray photoelectron spectroscopy (XPS) was performed on a VG Multilab 2000 system. The spectra were collected using Al Ka (1486.6 eV) radiation, and the overall energy resolution was about 0.45 eV. The single *C1s* peak was calibrated to 284.8 eV for all our samples.

2.3. Reaction test

The light-off testing and kinetic measurements were conducted in a packed-bed flow microreactor. Prior to each light-off test, the catalyst powders were heated in N_2 from RT to 100 °C in the reactor, then the sample was pretreated with 5% H_2/N_2 at 250 °C for 30 min and cooled down to 100 °C in N_2. To start the light-off test in a slightly lean condition (simulating lean-burn gasoline engine emission), the feed gas stream was switched to 5000 ppm CO- 500 ppm HCs (C_3H_6:C_3H_8 = 2:1)- 1.0% O_2- 5% H_2O- N_2 balance; 0.5 L/min; contact time: 1,500,000 $cm^3\ g_{cat}^{-1}\ h^{-1}$. The catalyst bed was first stabilized in the reaction gas stream at 100 °C for 30 min, and was then heated up to 350 °C at a ramping rate of 2 °C/min. Lower temperatures for the oxidation of CO and C_3H_6 translate into higher activity of the catalysts. The conversion of C_3H_8 was consistently zero below 350 °C. To calculate the apparent activation energies of CO and C_3H_6 oxidations, the measurement of the steady-state reaction rate began at the highest reaction temperature and lasted for 2 h before cooling to lower testing temperatures (hold for 1 h at each target temperature). As the last step of the reaction rate measurement, the reaction temperature was ramped up to the highest steady-state reaction temperature to confirm the repeatability. A typically 20 mg sample diluted with 200 mg of quartz sand was used to ensure that the heat transfer issue is dampened. The reactor tube has a diameter of 5 mm and length of 20 mm to avoid short channeling. Over- or unstable- heating due to the exothermic reaction is avoided by placing the thermocouple at front- and mid- catalyst bed to check for possible temperature gradients and turbulences. The film diffusion resistance was excluded by changing the flow rate with the fixed amount of catalyst, until a constant reaction rate was achieved, in that a high contact time (1,500,000 $cm^3\ g_{cat}^{-1}\ h^{-1}$) has been used. The overall conversion has been held under 20% to avoid the significant contribution from mass transfer during the kinetic measurement. A detailed quantitative estimation of the avoided pore diffusion impact for our catalytic reaction was shown in the SI (the pore diffusion issue). The same reaction gas atmosphere was used as a starting/ending feed stream condition for checking the CO oxidation reaction orders at 200 °C. To measure the reaction orders, the CO concentration was adjusted from about 1000 to 10,000 ppm, and the O_2 concentration was adjusted from 0.5 to 2%, respectively. Another set of light-off tests with a typical high oxygen concentration (500 ppm CO- 500 ppm HCs- 500 ppm NO- 5.0% O_2- 5% H_2O- N_2 balance; 100–350 °C; ramping rate 2 °C/min; contact time: 1,500,000 $cm^3\ g_{cat}^{-1}\ h^{-1}$) was used to simulate the catalytic conversion of diesel engine exhaust. Lower temperatures for the oxidation of CO, C_3H_6, and NO represent the more desired

activity of the catalysts. The intentional formation of NO_2 is to accelerate the selective catalytic reduction of NO_x located downstream of the emission control systems [36]. The feed and product gas streams were analyzed by a Nicolet 6700 FTIR equipped with an MCT detector and 3 m gas cell. The gas concentrations of H_2O, CO, CO_2, C_3H_6, C_3H_8, NO, NO_2, and N_2O were monitored in every 9 s. The carbon and nitrogen balances were closed in the repeated tests, and the formation of NH_3 and N_2 was not observed at any noticeable level. The kinetics measurement error was below 10%. The presence of HCs and steam each brought less than 5% difference to the measured reaction rates. Even without any O_2 present in the feed gas stream, the water-gas shift reaction did not happen at any noticeable level until above 270 °C.

3. Results and discussion

3.1. Improved catalytic performance driven by high and stable Pt dispersion

The overall structural properties and Pt dispersions of the various catalysts are summarized in Table 1. The Pt dispersion of 77% for the fresh 0.5 Pt/La-Al_2O_3 catalyst implies an overall fine dispersion of the supported Pt species. However, a severe Pt sintering in the aged 0.5 Pt/La-Al_2O_3 catalyst took place during the hydrothermal aging, where the platinum dispersion decreased to 24% from 77%. Agreeing with the literature [23], the well-dispersed Pt species don't have adequate sinter-resistant performance on La-Al_2O_3 support. Excitingly, there are almost 100% dispersions of Pt in both fresh and aged 0.4Pt-Ba/La-Al_2O_3 catalysts, highlighting the profound stabilization effect of Ba additives to the Pt during the hydrothermal aging. Even at higher Pt loadings, the aged 1.4Pt-Ba/La-Al_2O_3 catalyst shows a Pt dispersion of 36%, which is still about two times higher than the corresponding aged 1.5 Pt/La-Al_2O_3 counterpart. This group of number also teaches us that the maximal capacity of the current catalysts support to carry the fully dispersed Pt should be around 0.5 wt.%. We therefore designed our key samples using such a practical loading in the following work.

The XRD patterns for the representative aged catalysts are shown in Fig. 1. The baseline catalyst, aged 1.5Pt/La-Al_2O_3, is used as a reference to clearly show the diffraction peaks of Pt metal. After hydrothermal aging at 650 °C, the alumina support remains a complete γ phase in all the catalysts. However, sharp diffraction peaks of Pt metal show up in the aged 0.5Pt/La-Al_2O_3 catalyst, suggesting the severe sintering of the originally fine dispersed platinum species into metallic Pt particles. In contrast, the aged 0.4Pt-Ba/La-Al_2O_3 catalyst does not show any platinum metal crystals from XRD, and the introduction of Ba additives also doesn't bring any noticeable modifications to the alumina support. This again indicates that the Ba additives stabilize the Pt species by inhibiting the Pt sintering.

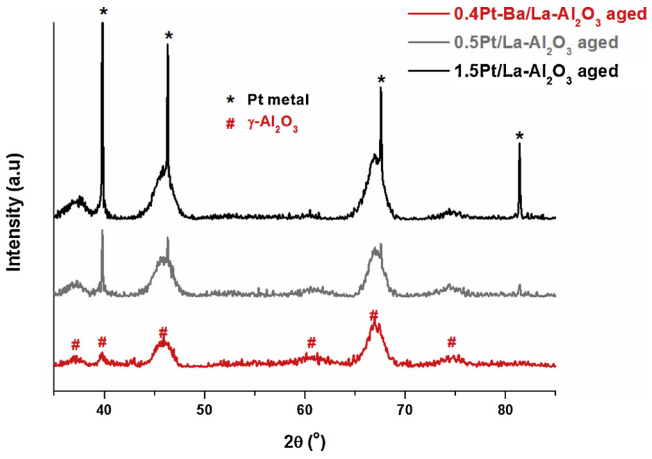

Fig. 1. The XRD patterns of the aged Pt/La-Al_2O_3 and Ba-stabilized- platinum catalysts.

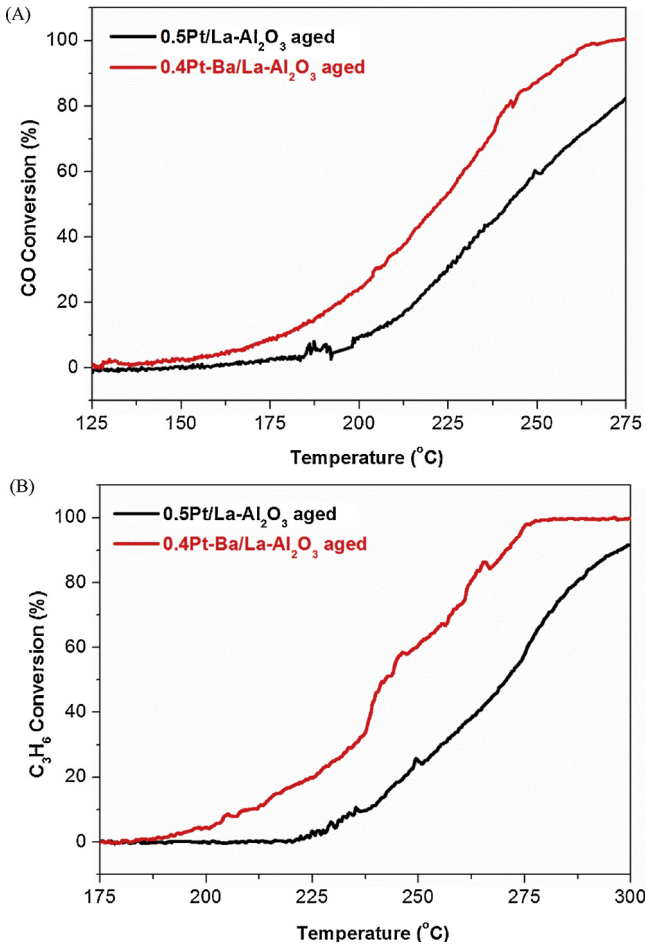

Fig. 2. The light-off conversion profiles of (A) CO oxidation and (B) C_3H_6 oxidation for the representative aged catalysts. Reaction condition (simulated lean-burn gasoline condition): 5000 ppm CO- 500 ppm HCs- 1.0% O_2- 5% H_2O- N_2 balance; 100–350 °C; ramping rate 2 °C/min; three consecutive light-off cycles; contact time: 1,500,000 $cm^3\ g_{cat}^{-1}\ h^{-1}$.

Next, we tested the catalytic performance of the representative aged catalysts in a simulated lean-burn gasoline engine emission. A set of light-off concentration profiles for the CO and C_3H_6 oxidation are shown in Fig. 2. It turns out that the aged catalyst with barium components is indeed more active than the catalyst without Ba for the conversion of CO and C_3H_6, and the extent of the activity improvements is positively correlated with the improved Pt dispersion (Table 1). Noted that although the improved reaction rate and turnover frequency (TOF) are among the highest values reported in the literature [37], the absolute temperatures for reaching a certain conversion are not as low as in a few other reports [17,37]. This is because a high contact time (20 mg sample, 0.5 L/min feed gas stream, contact time: 1,500,000 $cm^3\ g_{cat}^{-1}\ h^{-1}$) has been used to reflect the real-world operation conditions.

To further confirm the stability of the catalysts with and without Ba additives, the cyclic aging-tests under simulated diesel engine emission conditions were conducted on the two representative samples, as shown in Fig. 3. The platinum catalytic sites in the fresh 0.4Pt-Ba/La-Al_2O_3 sample stays stable during the course of the reaction up to aging temperatures for multiple cycles and over 48 h, while the accumulated catalytic capability of the fresh 0.5Pt/La-Al_2O_3 sample deteriorates after the extensive exposure to reaction atmosphere and high-temperature spikes, indicating the good stability of Ba additive sample. The light-off activity and stability tests illustrated the advantage of Ba-stabilized Pt catalyst for the pollutant purification reaction in typical types

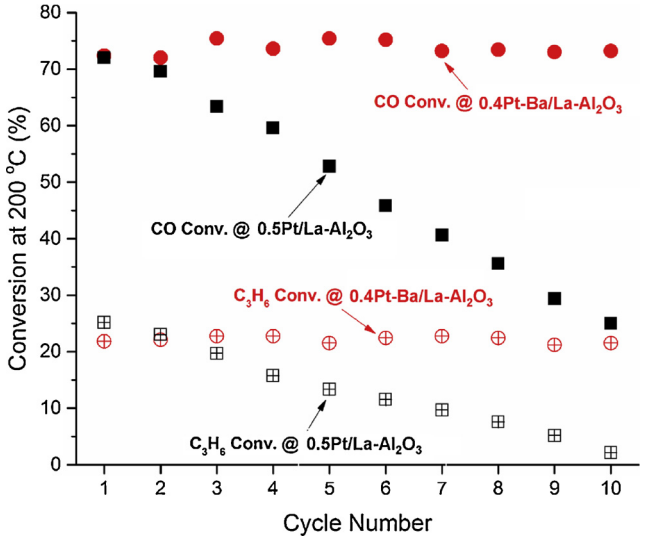

Fig. 3. Simulated lean-burn diesel emission steady-state cyclic tests of CO and C_3H_6 conversions at 200 °C after the fresh catalysts being exposed to the aging temperature of 650 °C for 30 min in reaction atmosphere (500 ppm CO- 500 ppm HCs- 500 ppm NO- 5.0% O_2- 5% H_2O- N_2 balance; ramping rate 10 °C/min; ten consecutive test cycles; contact time: 1,500,000 $cm^3\ g_{cat}^{-1}\ h^{-1}$).

of lean-burn engine emissions.

Kinetic measurements were conducted to probe the true active Pt sites for CO and C_3H_6 oxidation, as shown in Fig. 4A & B, and the corresponding catalytic performance comparisons are summarized in Table 2. Interestingly, similar E_a of 86 and 106 kJ/mol for the respective CO and C_3H_6 reaction has been observed in all the investigated catalysts (the activation energy numbers are close to those values previously reported [38–40]), indicating the addition of barium stabilizers and the evolution of sintered Pt structures would not change the overall reaction route. With a closer observation on the activity, we found the fresh 0.5Pt/La-Al_2O_3 exhibits similar CO and C_3H_6 oxidation activity, compared with the featuring 0.4Pt-Ba/La-Al_2O_3 samples, indicating the overall catalytic performance of the Pt/La-Al_2O_3 (with or without barium stabilizers) catalysts is determined by only one dominant type of platinum active site, that is, the dispersed platinum. After hydrothermal aging at 650 °C for 2 h, the activity of the aged 0.4Pt-Ba/La-Al_2O_3 catalyst remains similar with the fresh counterpart, while it decreases dramatically for the aged 0.5Pt/La-Al_2O_3 catalyst, and the drop of catalytic activity is directly associated with the dramatic decrease of Pt dispersion (Table 1). Compared with the hydrothermally aged 0.5Pt/La-Al_2O_3 catalyst that carries a similar amount of platinum, the 0.4Pt-Ba/La-Al_2O_3 catalyst triples the amount of the actual exposed platinum surfaces, and this translates into three times faster CO oxidation rate and ten times faster C_3H_6 oxidation rate (due to the increasing availability of Pt sites and less competition from the prioritized CO oxidation reaction). This indicates that the La-Al_2O_3 support alone was not fully adequate to stabilize the full dispersion of Pt during hydrothermal aging. A linear relationship between the CO oxidation reaction rates and the amount of the exposed Pt surfaces measured by CO chemisorption was also confirmed, indicating the active sites is indifferent to the presence of barium additives (Fig. 4C).

Reaction order tests were also performed to further probe the properties of platinum active sites and confirm the effect of barium additives, as shown in Fig. 5. The baseline Pt/La-Al_2O_3 catalysts and the sinter-resistant Pt-Ba/La-Al_2O_3 catalysts share the same reaction orders: 0.49 and 0.43 for CO and O_2 respectively. Therefore, we can conclude that the barium additives will not change the nature of the Pt catalytic center on La-Al_2O_3. There must be a common dominant catalytic site in both catalysts that steers the CO and C_3H_6 oxidation reactions. Being different in a classic Pt/Al_2O_3 system for CO oxidation, it has been well

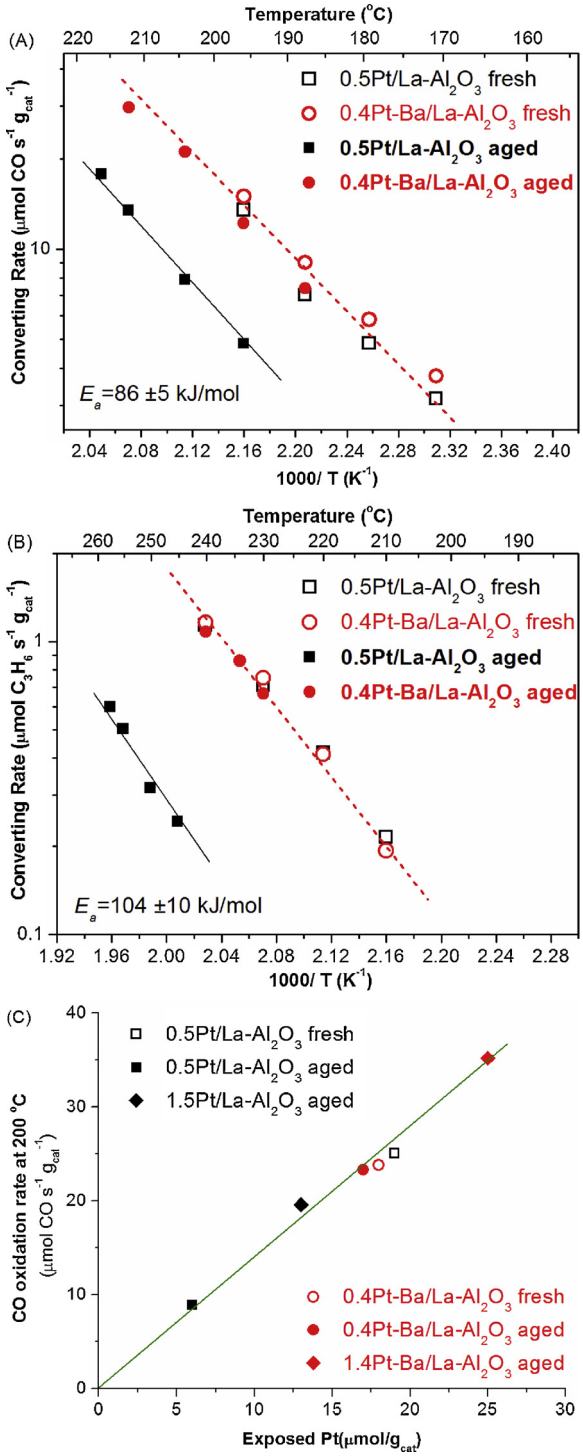

Fig. 4. Different catalytic performance but same intrinsic activity of the various platinum catalysts. Arrhenius plots of (A) CO oxidation reaction rates and (B) C_3H_6 oxidation rates in simulated lean-burn emission condition (5000 ppm CO- 500 ppm HCs- 1.0% O_2- 5% H_2O- N_2 balance; contact time: 1,500,000 $cm^3\ g_{cat}^{-1}\ h^{-1}$) of the fresh and aged catalysts. The similar apparent activation energies (*Ea*) for each reaction were shown in the figures. (C) A linear relationship between the CO oxidation reaction rates and the amount of the exposed Pt surfaces measured by CO chemisorption.

documented that the reaction orders for CO and O_2 are near -1 and 1 respectively [41]. Our internal work on Pt/Al_2O_3 catalysts also confirmed the reaction orders are -0.8 ~ -1.1 and 0.7 ~ 1.1 for CO and O_2 respectively. Therefore, we are not arguing against the classic wisdom

Table 2
Key chemical properties and catalytic behaviors of the baseline Pt/La-Al_2O_3 and the Pt-Ba/La-Al_2O_3 catalysts.

Samples	*Ea* (kJ/mol)*		Reaction orders*		State of Pt†	Converting rate*	
	CO oxidation	C_3H_6 oxidation	CO	O_2		CO	C_3H_6
0.5Pt/La-Al_2O_3 fresh	86 ± 5	104 ± 10	0.49	0.43	atomic Pt_1O_x- only	3× faster	10× faster
0.5Pt/La-Al_2O_3 aged					atomic Pt_1O_x-; bulky Pt^0 NPs	1×	1×
0.4Pt-Ba/La-Al_2O_3 fresh					atomic Pt_1O_x- only	3× faster	10× faster
0.4Pt-Ba/La-Al_2O_3 aged					atomic Pt_1O_x- only	3× faster	10× faster
1.5Pt/La-Al_2O_3 aged					–	–	–
1.4Pt-Ba/La-Al_2O_3 aged					–	–	–

*The kinetics were measured in a simulated lean-burn emission condition (5000 ppm CO- 500 ppm HCs- 1.0% O_2- 5% H_2O- N_2 balance; contact time: 1,500,000 $cm^3 g_{cat}^{-1} h^{-1}$). The reaction orders were determined at 200 °C by adjusting the CO and O_2 concentrations in the above gas mixture and limiting the overall CO conversion below 20%. †A conclusion combining Pt dispersion (by CO chemisorption), Pt morphology (by HAADF-STEM), and Pt coordination chemistry (by XAS) results. The values shown at the front of sample labels are wt.% Pt.

in this work, but reporting the new findings as the current benchmark Pt/La-Al_2O_3 catalysts no longer behave in the exact same way as we learned from the classic Pt/Al_2O_3 system. We consider the key differences are attributed to the nature of catalytic center as isolated cationic Pt that leads to weaker CO adsorption [42,43], likewise to Pd [9,44], the presence of H_2O in the reaction that moderates the CO inhibition on Pt [45,46], and the presence of C_3H_6 that competes with CO for Pt sites [47,48]. A more detailed discussion of the measured kinetic parameters and their implication to the catalytic route for the given material system will be discussed later in the paper, after the true catalytic center and its intrinsic activity have been explicitly identified.

Notably, increasing the platinum loading to 1.4Pt-Ba/La-Al_2O_3 resulted in minor improvement over the baseline 1.5Pt/La-Al_2O_3 catalyst. This is because in both catalysts the capacity to disperse atomically the Pt had been exceeded, as indicated by the presence of aggregated platinum nanoparticles (Pt not fully dispersed) identified by CO chemisorption (Table 1). In these samples, the number of exposed Pt atoms estimated by CO chemisorption was between 13–25 μmol/g_{cat}, meaning that an ideal sinter-resistant catalyst bearing a 0.3-0.5 wt.% of fully dispersed platinum active sites would catalyze the reactions equally well.

3.2. Retaining the atomically dispersed Pt species leads to high Pt dispersion

The HAADF-STEM figures for fresh 0.5Pt/La-Al_2O_3 and 0.4Pt-Ba/La-Al_2O_3 catalysts are shown in Fig. 6. It is observed that there are no discrete large nanoparticles at low magnifications (Fig. 6A & C, inset) in either catalysts, as their high measured Pt dispersion already indicated. An abundance of atomically dispersed elements shows up at high magnifications in both samples. The contrast of the atomic species in HAADF-STEM is approximately in proportion to the square of the atomic numbers for each element in the periodic table. Compared with platinum atoms, the lanthanum and barium atoms are about two times lower in contrast, but much brighter than alumina support. Therefore, it is probable that the isolated atoms with slightly lower contrast are the lanthanum ions or the barium additives on the alumina surface [49,50]. However, their presence doesn't disguise the existence of the atomically dispersed platinum, which should be shown as the brighter dots and there are no Pt particles in those samples to potentially contribute to any alternative form of Pt presence. A few sub-nm clusters without showing any organized crystal planes are also observable at high magnifications, especially on the fresh 0.5Pt/La-Al_2O_3 catalyst, but the rare presence of these small clusters does not seem to be the prevalent Pt species either. To further confirm this, CO chemisorption shows that the Pt was measured to have close to 100% dispersion for the fresh 0.4Pt-Ba/La-Al_2O_3 catalyst (Table 1), indicating the Pt sites must be fully dispersed species. Therefore, we estimate that the Pt mostly retains atomically dispersed in the fresh 0.5Pt/La-Al_2O_3 and 0.4Pt-Ba/La-Al_2O_3 catalysts. XAS analysis will further confirm that the atomically dispersed platinum species are the dominant components in the two fresh samples (see latter discussion for XAS data).

After hydrothermal aging at 650 °C for 2 h, large nanoparticles with a size range from 20 to 300 nm are observed in the aged 0.5Pt/La-Al_2O_3 catalyst (Fig. 7A & B, inset). The EDS analyses on those large particles

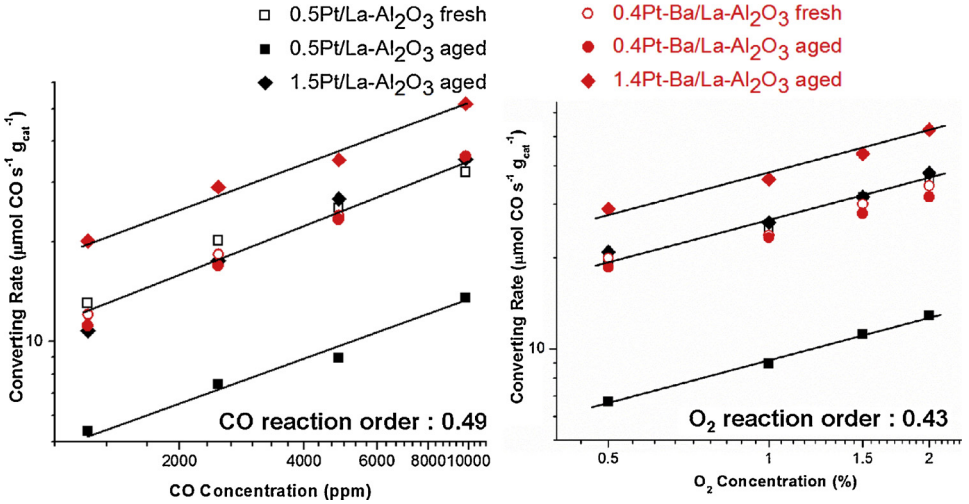

Fig. 5. The measurement of the CO and O_2 reaction orders by rate law. Feed gas: 5000 ppm CO- 500 ppm HCs- 1.0% O_2- 5% H_2O- N_2 balance as the starting/ending gas feed stream to check repeatability; 200 °C; 5 L/min; CO conversion < 20%.

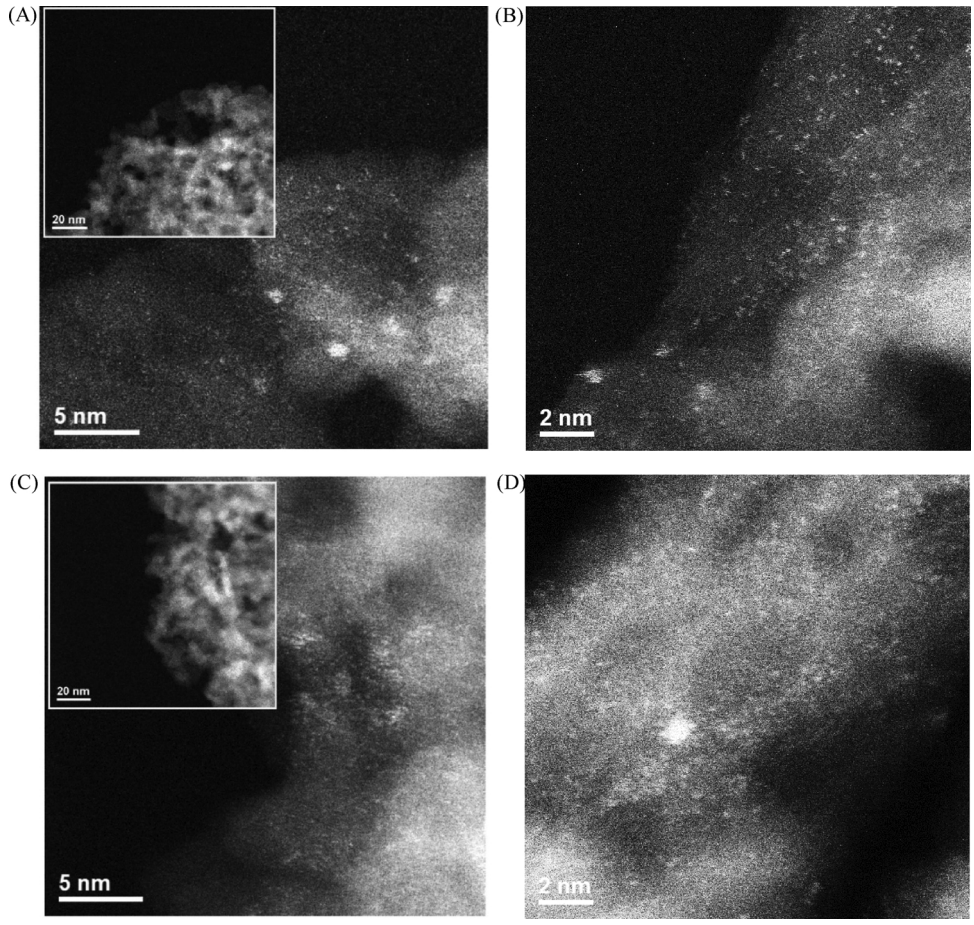

Fig. 6. A typical series of HAADF-STEM images of the fresh (A)(B) 0.5Pt/La-Al_2O_3 and (C)(D) 0.4Pt-Ba/La-Al_2O_3 catalyst showing few sub-nm platinum clusters and primarily (count frequency > 95%) atomically dispersed platinum species (0.2-0.3 nm). Note scale markers.

show that the large aggregates are Pt metal only, rather than any possible new compounds forming with other element such as La and oxygen (Fig. 7C). This is consistent with the detection of large Pt metal crystals in XRD (Fig. 1). Indeed, the dramatically lower Pt dispersion of 24% for the aged 0.5Pt/La-Al_2O_3 catalyst implies the sintering of well dispersed Pt atoms (Table 1). However, we found that the well-established theoretical relation between the metal crystal size and metal dispersion (Particle Diameter (nm) ≈ 1/Dispersion (%)) [51] could not explain why the aged 0.5Pt/La-Al_2O_3 catalyst with platinum particle sizes from 20 to 300 nm retains 24% platinum dispersion. To our surprise, the microscopy results at atomic resolution reveal the possible presence of the atomically dispersed platinum species on the surfaces of the aged 0.5Pt/La-Al_2O_3 catalyst (Fig. 7A & B), and XANES and EXAFS analyses will confirm the existence of such atomically dispersed platinum (see XAS analysis in latter sections). Note that we didn't find any sizes in between the single atoms and large particles after aging. Previous work from Datye's group [9,44] also found that such a La-Al_2O_3 support is particularly capable in creating the atomically dispersed PGM species even through conventional incipient wet impregnation synthesis. However, in terms of sintering resistance, the work from Datye's group also found that the Pd single atoms tend to sinter easily even at very mild reaction temperatures (100 °C), and thus jeopardized the CO oxidation catalytic activity instantly [9]. We therefore conducted a systematic study on this subject to deliver a refreshed consideration of the Pt/La-Al_2O_3 catalysts by revealing what the Pt species are on the very support and which of them are active in a context of applied catalysis. As an extra step, we tried to stabilize the highly active sites that can otherwise sinter severely. Encouragingly, all the platinum remains atomically dispersed in the aged 0.4Pt-Ba/La-Al_2O_3 catalyst, and no sintered platinum particles are observed in any STEM images (Fig. 7D & E), agreeing well with the CO chemisorption results (Table 1). Regarding to the homogeneity of our single atoms, it has a lower extent of homogeneity than the more fundamental-oriented studies recently reported [52,53] due to our higher Pt loadings (~0.5 wt. %). As shown in Fig. S3, the CO adsorption peak at ~2105 cm^{-1} can be attributed to the adsorption on the cationic Pt single atoms, and the FWHM of the IR is about 30 cm^{-1}. This value is clearly larger than the 6-8 cm^{-1} reported by Christopher's group on the highly clean system of one Pt atom on each TiO_2 particle [52], confirming the lower extent of homogeneity of the obtained application-oriented Pt single atoms. However, our FWHM of the aged sample is still largely in par with many other single-atom Pt on CeO_2 (~35 cm^{-1}, [54]), FeO_x (~35 cm^{-1}, [8]), m-Al_2O_3 (~25 cm^{-1}, [17]) and HZSM-5 (~25 cm^{-1}, [16]), corroborating the legitimate detection of the single-atom dominating nature in our sinter-resistant Pt-Ba/La-Al_2O_3 formulation.

3.3. The chemical environment of the single-atom Pt species and the stabilization of the Pt by -O_x-Ba stabilizers

The XAS results help us to confirm that the surface –O- linkages are the species to keep the platinum catalytic sites atomically dispersed. For the as-received catalysts, the XANES data (Fig. 8A) reveals that cationic Pt(IV) ions are the major platinum components in the fresh Pt/La-Al_2O_3 and Pt-Ba/La-Al_2O_3 catalysts, all of which have high Pt dispersion (Table 1). The difference between the Pt/La-Al_2O_3 and the sinter-resistant Pt-Ba/La-Al_2O_3 catalysts shows up after the hydrothermal aging. The decrease of the XANES white line intensity for the aged 0.5Pt/La-Al_2O_3 and 1.5Pt/La-Al_2O_3 catalysts indicates the reduction of the Pt

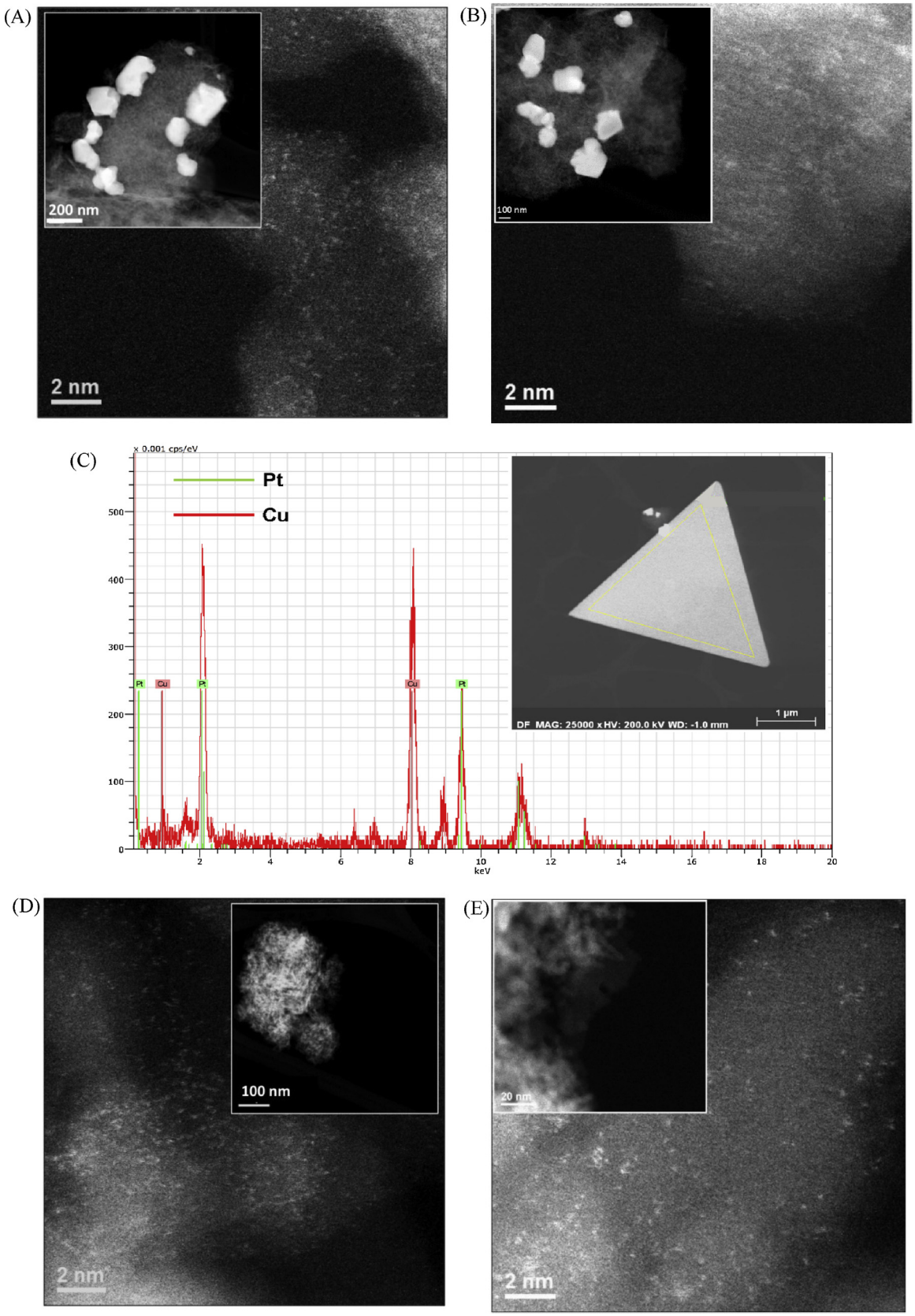

Fig. 7. A typical series of HAADF-STEM images of (A)(B) the hydrothermally aged 0.5Pt/La-Al_2O_3 showing the coexistence of sintered platinum particles and a few atomically dispersed sites, (C) EDS analysis for the huge nanoparticles in the hydrothermally aged 0.5Pt/La-Al_2O_3, and (D)(E) hydrothermally aged 0.4Pt-Ba/La-Al_2O_3 catalyst showing mostly (count frequency > 98%) atomically dispersed platinum species (0.2-0.3 nm). Note scale markers.

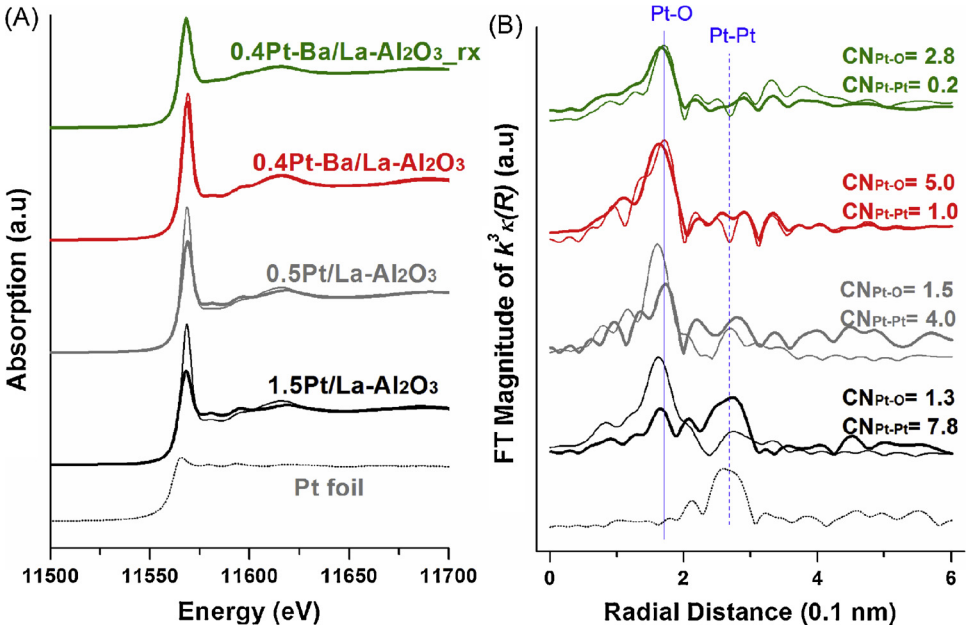

Fig. 8. The XAS analysis of the supported platinum components. (A) XANES and (B) EXAFS results of the as-received and reaction-spent (sample name ends with "rxn") catalysts (5000 ppm CO- 500 ppm HCs- 1.0% O_2- 5% H_2O- N_2 balance; 100–350 °C; ramping rate 2 °C/min; three consecutive light-off cycles; contact time: 1,500,000 $cm^3\ g_{cat}^{-1}\ h^{-1}$); fresh samples in thin line; aged samples in bold line. Listed coordination numbers are for aged samples; see Table 3 for details of the fitting parameters.

ions. Such a trend is accompanied by the parallel EXAFS results shown in Fig. 8B, where a clear transition of Pt-O to Pt-Pt bond in the aged 0.5Pt/La-Al_2O_3 and 1.5Pt/La-Al_2O_3 catalysts can be tracked. These findings are in agreement with the formation of sintered platinum metal particles observed by CO chemisorption and XRD (Table 1 and Fig. 1). Notably (and consistent with the HAADF-STEM findings for the aged Pt/La-Al_2O_3 catalysts), there is still a remaining feature of Pt-O bond representing the dispersed platinum species in those aged Pt/La-Al_2O_3 catalysts. Therefore, the platinum components in the aged Pt/La-Al_2O_3 catalysts have a bimodal size distribution, comprising the dispersed atoms plus particles.

A full list of coordination conditions obtained by fitting the EXAFS data can be found in Table 3. The minimal Pt-Pt coordination contribution in the 0.4Pt-Ba/La-Al_2O_3 catalysts rules out any significant presence of the sintered Pt clusters or particles within the experimental/fitting error. For example, even with a 100% weighted contribution, a typical ~1 nm metal clusters will give a Pt–Pt coordination number about 4, and a Pt-Pt dimer will only give 1 as the Pt–Pt coordination number [55,56]. Therefore, the atomically dispersed Pt_1O_x- species must be the dominant components in those Pt/La-Al_2O_3 catalysts with and without Ba additives that have high Pt dispersion.

Table 3
Fitting parameters of the curve fitted k^3-weighted EXAFS analysis of the as-received and reaction-spent platinum catalysts*.

Sample	Shell	N	R(Å)	ΔE_0 (eV)	R-factor
1.5Pt/La-Al_2O_3 fresh	Pt-O	4.30	2.00	7.29	0.04
	Pt-Pt	0.66	2.75		
1.5Pt/La-Al_2O_3 aged	Pt-O	1.26	1.97	6.90	0.03
	Pt-Pt	7.76	2.76		
0.5Pt/La-Al_2O_3 fresh	Pt-O	4.46	1.99	8.55	0.03
	Pt-Pt	0.96	2.74		
0.5Pt/La-Al_2O_3 aged	Pt-O	1.47	2.04	9.20	0.04
	Pt-Pt	3.97	2.81		
0.4Pt-Ba/La-Al_2O_3 fresh	Pt-O	5.22	2.00	8.76	0.04
	Pt-Pt	0.75	2.88		
0.4Pt-Ba/La-Al_2O_3 aged	Pt-O	5.08	2.00	9.45	0.04
	Pt-Pt	1.06	2.69		
0.4Pt-Ba/La-Al_2O_3 fresh_rxn	Pt-O	2.53	2.03	9.03	0.03
	Pt-Pt	0.63	2.63		
0.4Pt-Ba/La-Al_2O_3 aged_rxn	Pt-O	2.75	2.01	7.49	0.03
	Pt-Pt	0.21	2.83		

* Amplitude reduction factor S_0^2: 0.90; N, coordination number; R, distance between absorber and backscattered atoms; ΔE_0, inner potential correction; R-factor, closeness of the fit, if < 0.05, consistent with broadly correct models. Estimated error: N: ± 20%, R: ± 0.03; ΔE_0: ± 25%.

With the platinum atoms fully dispersed and their intrinsic activity intact, the 0.4Pt-Ba/La-Al_2O_3 catalysts serve as an excellent platform to understand the nature of the active platinum sites on alumina-based materials. The XANES analysis of the Pt L_{III} edge for the reaction-spent catalysts (three consecutive light-off cycles up to 350 °C) shows that the platinum stays as Pt(II) in both fresh and aged 0.4Pt-Ba/Al_2O_3 catalysts (Fig. 8A). The corresponding Pt-O coordination number decreases by about 50% without any simultaneous Pt-Pt bond formation (Fig. 8B). Therefore, the change of the coordination condition is not due to the platinum sintering, but due to the self-adaptation of the catalytic center to the pretreatment and reaction condition. Whether the 0.4Pt-Ba/La-Al_2O_3 catalysts have been aged will not alter this observation. In the reaction-spent 0.4Pt-Ba/La-Al_2O_3 catalysts, the single catalytic center structured as Pt(II)-O_x- (x ≈ 2–3) (Fig. 8 and Table 3) matches with the computational models constructed by Moses-DeBusk *et al.* very well [57]. The first-principles DFT study proposed that a Pt-oxo- structure was the highly active site for the CO oxidation, where the alumina substrate was not part of the catalysis. In fact, the similarly structured Pt-oxo- sites were also experimentally found on KLTL zeolites [7] and FeO_x [8], both of which were designed for CO oxidation below 150 °C.

For the sinter-resistant 0.4Pt-Ba/La-Al_2O_3 catalysts, the hydrothermal aging treatment did not change the overall chemical valence of the cationic platinum species, according to the XANES data. The corresponding EXAFS data (Fig. 8B and Table 3) for the fresh and aged 0.4Pt-Ba/La-Al_2O_3 catalysts also shows that there is essentially no change of the Pt-O coordination condition. This demonstrates that the atomically dispersed platinum species is adequately stabilized by the nearby oxygen linkages in the 0.4Pt-Ba/La-Al_2O_3 catalyst.

The XPS analysis for Ba *3d* (Fig. 9) shows that barium additives have a stable chemistry in all the 0.4Pt-Ba/La-Al_2O_3 catalysts before and after the reaction. The Ba *3d* peak position alone may not precisely reveal if the barium ions were associated with carbonates or –O- linkages, but the presence of the carbonates species (corresponding C*1s* peak located at 289.1 to 290.8 eV [58]) was excluded by the C*1s* single peak location (always near 284.8 eV) and XRD results (Fig. 1). Therefore, it is the –O_x-Ba linkage that facilitates the stabilization of the atomically dispersed platinum species on alumina support. These chemical linkages to Pt have been proved to be more stable than the

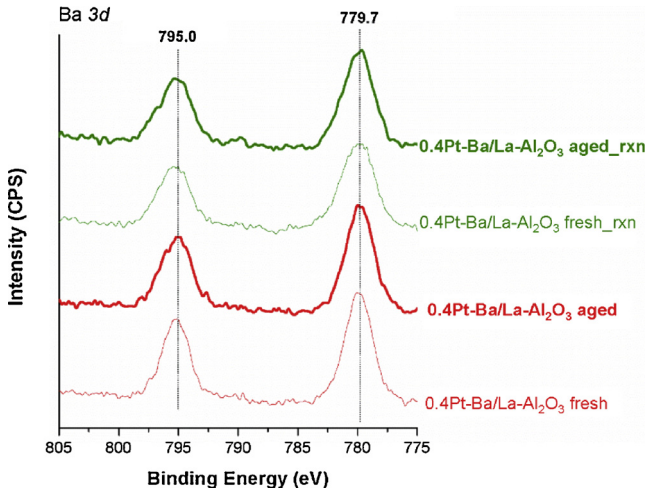

Fig. 9. The Ba *3d* XPS of the as-received and reaction-spent Ba-stabilized catalysts. Reaction condition: 5000 ppm CO- 500 ppm HCs- 1.0% O_2- 5% H_2O- N_2 balance; 100–350 °C; ramping rate 2 °C/min; three consecutive light-off cycles; contact time: 1,500,000 $cm^3\ g_{cat}^{-1}\ h^{-1}$.

previously reported Pt–O_x-La linkages [24] to survive the hydrothermal aging. The most surprising is that with the stabilization of –O_x-La and –O_x-Ba linkages together, the Pt-O_x coordination condition changes during reaction but still inhibits the aggregation from single atoms to nanoparticles (Fig. 8B and Table 3).

The activation and Pt-O_x coordination condition similarities on fresh catalysts with and without Ba indicate that the impact of barium is indirect in defining the catalytic Pt center (Fig. 4A & B, Table 3). After looking at more Pt/La-Al_2O_3 and Pt-Ba/La-Al_2O_3 catalysts, we found that the addition of tiny amounts of barium did not change the apparent activation energy (Fig. 4A & B, Table 2), reaction orders (Fig. 5), nor the alumina texture (Table 1) in either fresh or aged states, but survived the catalytic center in cyclic aging tests (Fig. 3). The linear relationship between the CO oxidation reaction rates and the amount of the exposed Pt surfaces measured by CO chemisorption also demonstrate that the active sites have no relevance to the barium additives (see Fig. 4 C). These results unequivocally show that the effect of barium is catalytically indirect — the barium additives are the stabilizers for the original active platinum catalytic center on La-alumina.

3.4. Sintered Pt particles are not the true catalytic domain in CO and C_3H_6 oxidation reactions

To validate our estimation based on various experimental observations that the atomic Pt_1O_x- species are the catalytic center for the Pt/La-Al_2O_3 catalysts with and without Ba, we need to quantify the number of the platinum single atoms and metal particle surface atoms in each catalyst firstly. Counting of the single atoms in HAADF-STEM figures is a good method, but we can't distinguish the exact platinum single atoms in the presence of La and Ba sites due to the resolution limit of EDS. However, for those Pt/Al_2O_3 catalysts that carry the exclusive (or mostly) Pt_1O_x- species on alumina, the exact Pt-O coordination condition can be determined by EXAFS, without the undesired interference from sintered metal particles. Considering the interferences from CO and −OH adsorption under reaction conditions, we use the data from the as-received catalysts without being exposed to reactions to more precisely quantify the various sites. This "calibrated" result will help us to determine the volume weight of the same atomic Pt_1O_x- species in other Pt/Al_2O_3 catalysts comprising sintered particles. From the Pt(IV)O_2 film and Ba_4Pt(IV)O_6 Feff models we adopted for EXAFS fitting, the stable platinum atoms were found to complex with six surrounding oxygen atoms. From the EXAFS analysis data (Table 3), the actual Pt(IV)-O coordination numbers are above 5 in the as-received 0.4Pt-Ba/La-Al_2O_3 catalysts, but the minor Pt-Pt bond contributions must have brought down the average Pt-O coordination number slightly. According to this evidence, the atomically dispersed platinum atoms on alumina are most likely coordinating with six 1st shell oxygen atoms, and this will be the calibrated structure for any atomic Pt_1O_x-species in the as-received catalysts. For the platinum metallic particles, Miller et al. revealed the relation between the Pt-Pt coordination number and the number of exposed platinum atoms of a given metallic particle systematically [55], we can estimate the number of surface platinum atoms on the sintered particles by the volume-weight-adjusted EXAFS fitting numbers. Therefore, we can statistically estimate the population of the Pt atoms staying either as atomically dispersed species or residing on the surface of the sintered metallic particles with volume-weight of each species been adjusted. The following relations between the measured value and the portion of the different platinum sites have been used:

$$Measured\ CN_{Pt-O} = (Standard\ CN_{Pt-O}\ of\ PtO_2\ film) \times (Mole\ \ Ratio\ of\ the\ Atomic\ Pt_1O_x)$$

$$Pt\ \ Dispersion\ from\ Pt_1O_x\ Contribution\ (\%) = (Mole\ Ratio\ of\ \ the\ Atomic\ Pt_1O_x) \times 100$$

$$Measured\ CN_{Pt-Pt} = \sum_{Single\ Atom}^{Nanoparticle} (Mole\ Ratio\ of\ Pt) \times (True\ \ CN_{Pt-Pt})$$

$$Pt\ Dispersion\ from\ Pt^0\ Particle\ Contribution\ (\%) = (Mole\ Ratio\ of\ the\ Pt\ as\ Metallic\ Particles) \times 10^{-0.130(\pm0.005)\times(True\ \ CN\ _{Pt-Pt})+2.58(\pm0.04)}$$

The quantified results for atomic Pt_1O_x- species and sintered platinum nanoparticles are summarized in Fig. 10. Next, we further casted the turnover frequency (TOF) by dividing the overall CO oxidation rate over the number of atomically dispersed platinum atoms from the Pt_1O_x- structure. The obtained TOFs stay similar for all the catalysts, around 1.35 s^{-1} at 200 °C, indicating the sinter-resistant Pt_1O_x- species is the true site catalyzing the CO and C_3H_6 oxidation on La-alumina (Fig. 10), not the sintered Pt particles. Our newly developed sinter-resistant Pt-Ba/La-Al_2O_3 catalysts are clearly one of the more active single-atom Pt catalysts using no-reducible supports [7,17,37]. In a broader scope of material choices, important recent work reported that

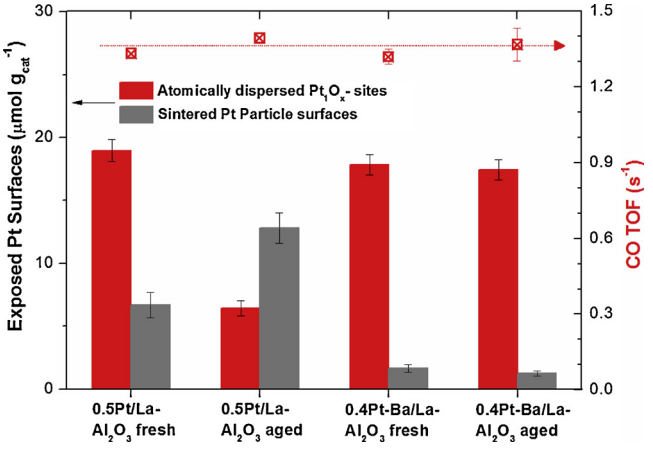

Fig. 10. Confirming the origin of the more active Pt species in CO oxidation. Quantification of the exposed Pt surfaces from atomic Pt_1O_x- species and sintered platinum particles. The tiny contribution of Pt-Pt bond in the 0.4Pt-Ba/La-Al_2O_3 samples was from EXAFS data fitting errors. The TOF was casted by dividing the overall reaction rate at 200 °C over the amount of atomically dispersed Pt atoms. Considering the interferences from CO and −OH adsorption under reaction conditions, we use the data from the as-received catalysts without being exposed to reactions to quantify the various sites.

the Pt/Al_2O_3 catalysts become highly active for CO oxidation at the optimal Pt particle size of 2–4 nm [59,60]. We extrapolated these reported activity data to our measurement conditions by taking both temperature and gas concentrations into consideration, and found the intrinsic activity per Pt site in these reported catalysts are within the same magnitude as our best samples have (0.20–0.41 s^{-1} in [59,60] and 1.35 s^{-1} in our case). A detailed calculation of those results was included in SI (the TOF comparisons). Since we won't be able to host an abundant presence of 2–4 nm Pt metal nanoparticles on the $La\text{-}Al_2O_3$ support in this work due to the material nature, we will not make a judging statement that whether the single-atom $Pt_1\text{-}O_x$ species is more active than the 2–4 nm Pt metal nanoparticles, despite the favoring numbers for the single atoms through the preliminary estimation. We hope to reiterate that the findings from our present work is not in conflict with the claims in literature, pointing that the low-coordinated and reactive surface Pt atoms [59] and the edge, terrace Pt atoms [60] can be highly effective catalytic components for the CO oxidation reaction. In our system, the alternative structure as $Pt_1\text{-}O_x$ simply provides a promising platform to retain a high intrinsic activity per Pt atom, and ensures a 100% Pt material utilization efficiency in the meantime. The latter cannot often be met through a typical Pt nanoparticle system, where not all the Pt atoms are exposed on the surface to catalyze reactions when the Pt particle size is larger than 1 nm. Notably, the thermal durability of our new single-site catalysts has been enhanced to tolerate much more demanding operation temperatures and realistic reaction atmosphere.

Moreover, compared with the more conventional Pt/ceria-based formulation that also improves PGM dispersion, our new $Pt\text{-}Ba/La\text{-}Al_2O_3$ catalysts are particularly advantageous to CO, C_3H_6, and NO oxidation in the lean-burn exhaust (Fig. 11). In agreement with other earlier reports [14,15], the $1.2Pt\text{-}Ce/La\text{-}Al_2O_3$ catalyst delivers inferior catalytic performance in the oxygen-rich atmosphere. Alternatively, if only testing the samples under a simple gas mixture near a stoichiometric condition: 1% CO- 0.5% O_2- 5% H_2O- N_2 balance (contact time: 1,500,000 cm^3 g_{cat}^{-1} h^{-1}), the aged $1.2Pt\text{-}Ce/La\text{-}Al_2O_3$ catalyst was able to reach 50% CO conversion near 150 °C, while the aged $1.5Pt/La\text{-}Al_2O_3$ catalyst could not reach 50% CO conversion until above 225 °C. These findings reinforce our view that developing a stable high dispersion $Pt/La\text{-}Al_2O_3$ catalyst is practically important, and the task cannot be circumvented by using ceria-based materials for the scenario of oxygen-rich reactions.

The above thread of single-atom catalysis does not necessarily rule out the possibility that a tiny portion of the sintered platinum nanoparticles, such as the coordination-unsaturated corner and perimeter platinum atoms [59,61], analogous to the palladium and gold nanoparticles [61–64], might be comparably active in catalytic reactions. Nonetheless, our finding unequivocally points out that the sintered platinum nanoparticles (20–300 nm) are predominantly a spectator species in the emission-cutting catalysis, although these particles often have major presence in various characterization results for automotive catalysts. Catalyst development merely focusing on mitigating sintered PGM particles may not produce optimal outcomes.

3.5. The implications from the kinetics of the single-atom catalysts

To probe the reaction mechanism indicated by our kinetic measurement, we proposed a possible reaction path and derived the rate equations. The reaction orders we measured indicate that both the CO

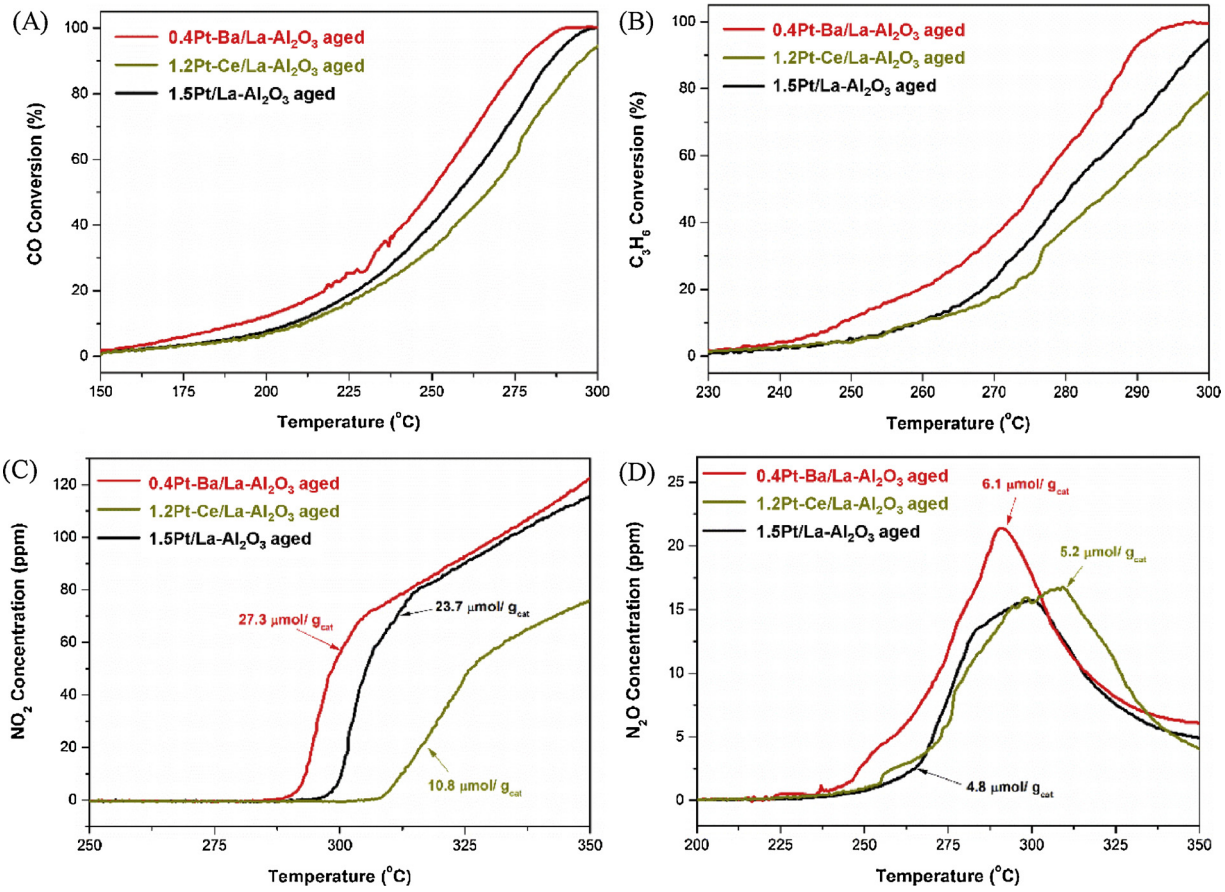

Fig. 11. Representative light-off reaction profiles for (A) CO conversion, (B) C_3H_6 conversion, (C) desired NO_2 formation, and (D) byproduct N_2O formation in simulated lean-burn engine exhaust (500 ppm CO- 500 ppm HCs- 500 ppm NO- 5.0% O_2- 5% H_2O- N_2 balance; 100–350 °C; ramping rate 2 °C/min; three consecutive light-off cycles; contact time: 1,500,000 cm^3 g_{cat}^{-1} h^{-1}.).

and O are the most abundant reaction intermediates during the reaction over our catalysts. Since the active catalytic center is single-atom Pt, rather than an extended Pt surface with multiple identical neighboring sites, we consider that CO and O_2 molecules will adsorb and be activated on distinctive sites. Namely, CO may adsorb on the single-atom Pt, while O_2 will adsorb and be activated on the Pt-O-support interface, being similar to what the single-atom Pd/γ-Al_2O_3 catalyst does [9]. Assuming the H_2O as a co-catalyst that can be canceled out in reaction steps, the simplified overall reaction route becomes:

$$CO + \sigma_1 \underset{k-1}{\overset{k1}{\rightleftharpoons}} CO(a)$$

$$O_2 + 2\sigma_2 \underset{k-2}{\overset{k1}{\rightleftharpoons}} 2O^*(a)$$

$$CO(a) + O^*(a) \xrightarrow{k3} CO_2(a) \xrightarrow{fast} CO_2$$

Where σ_1 is the CO adsorption site on Pt single atoms, σ_2 is the O_2 adsorption site on the Pt-O-support interface.

When CO adsorption, O_2 adsorption and dissociation reach equilibrium, the reaction rate can be:

$$r = \frac{K_1 k_3 P_{CO} \sqrt{K_2 P_{O_2}}}{(1 + K_1 P_{CO})(1 + \sqrt{K_2 P_{O_2}})}$$

$$K_1 = \frac{k_1}{k_{-1}} \quad K_2 = \frac{k_2}{k_{-2}}$$

Since the adsorption of O_2 is usually weak, thus

$$1 + \sqrt{K_2 P_{O_2}} \approx 1$$

$$r = \frac{K_1 k_3 P_{CO} \sqrt{K_2 P_{O_2}}}{(1 + K_1 P_{CO})}$$

We got an O_2 reaction order of ~0.5, which is consistent with the numbers we measured.

In terms of the positive reaction order for CO observed experimentally, it relies on the value of K_1 that is mitigated by the catalytic formulation and reaction gas conditions.

When K_1 is very large, $1 + K_1 P_{CO} \approx K_1 P_{CO}$, then

$$r = k_3 \sqrt{K_2 P_{O_2}}$$

The reaction order for CO will be 0.

To another extreme, when K_1 is close to 0, $1 + K_1 P_{CO} \approx 1$, then

$$r = K_1 k_3 P_{CO} \sqrt{K_2 P_{O_2}}$$

The reaction order for CO will be 1.

Therefore, the measured CO reaction order will land between 0 and 1 in an actual reaction. In this study, both the presence of water and C_3H_6 in our feed gases will weaken the adsorption of CO if compared with a scenario of a simple CO + O_2 reaction on a classic system of Pt metal nanoparticles supported on pure alumina [45–48]. In addition, from the perspective of our catalytic materials, the catalytic Pt center as single-atom cationic species in the Pt/La-Al_2O_3 formulation with or without Ba leads to weaker CO adsorption, as the high wavenumbers for CO-Pt IR peak (Fig. S3) and a few recent studies indicated [9,42–44]. Revisiting the kinetic rate equation, these factors discussed above contributed to the weakened CO adsorption together, resulting in a reasonably small K_1. A positive reaction order for CO therefore becomes feasible. This observation is of significant value for practical applications as well, as the positive reaction order of CO indicates a lower possibility of CO poisoning of PGM that inhibits the CO oxidation [41]. For the CO oxidation on the conventional Pt/Al_2O_3 catalysts, where the active sites were Pt metal nanoparticles, earlier work from General Motors R&D showed that a positive reaction order for CO becomes possible when CO concentration must be less than 400 ppm in the presence of 1% O_2 at 200 °C [65].

Regarding the similar E_a to the classic CO oxidation on Pt/Al_2O_3 catalysts, it should be simply a coincidence as both the chemistry of single-atom Pt catalytic center and the reaction orders for CO and O_2 are suggesting a different catalysis. The reaction environment and material's nature are both quite different from the classic Pt/Al_2O_3 studies performed in literature [38,66].

4. Conclusions

In this work, the otherwise highly unstable single-site Pt_1O_x- catalytic species on the La-alumina surface has been effectively stabilized by barium additives through surface oxygen linkages. The same active but more stable catalytic sites can survive in the reaction stream and hydrothermal aging up to 650 °C. We have demonstrated that the concept of heterogeneous single-atom catalysis applies to high operating temperatures, and using inert oxides such as alumina-based materials to carry those atomic catalytic centers is indeed possible. The knowledge garnered from this work may pave the way for implementing the concept of single-atom catalysis into various industrially important processes that operate in harsh reaction conditions.

Acknowledgements

The work from Tianjin Univ. was supported by the National Key Research and Development Program (2017YFC0211002), the Science and Technology Program of Tianjin (16YFZCSF00290), and the grant from GM Global R&D. Microscopy work at ORNL was supported by a Strategic Partnership Project funded by GM Global R&D, and in part by the U.S. Department of Energy (DOE), Office of Energy Efficiency and Renewable Energy, Vehicle Technologies Office, Propulsion Materials Program. This research used resources of the Advanced Photon Source, a US-DOE Office of Science User Facility operated for the DOE Office of Science by Argonne National Laboratory under Contract No. DE-AC02-06CH11357. The paper is dedicated to celebrating Tom Johnson' retirement after 40 years' research work at General Motors Global R&D.

Appendix A. Supplementary data

Supplementary material related to this article can be found, in the online version, at doi:https://doi.org/10.1016/j.apcatb.2018.11.034.

References

[1] M. Flytzani-Stephanopoulos, B.C. Gates, Atomically dispersed supported metal catalysts, Annu. Rev. Chem. Biomol. Eng. 3 (2012) 545–574.
[2] J.M. Thomas, Catalysis: tens of thousands of atoms replaced by one, Nature 525 (2015) 325–326.
[3] Y. Zhai, D. Pierre, R. Si, W. Deng, P. Ferrin, A.U. Nilekar, G. Peng, J.A. Herron, D.C. Bell, H. Saltsburg, M. Mavrikakis, M. Flytzani-Stephanopoulos, Alkali-stabilized Pt-OH_x species catalyze low-temperature water-gas shift reactions, Science 329 (2010) 1633–1636.
[4] M. Yang, L.F. Allard, M. Flytzani-Stephanopoulos, Atomically dispersed Au–$(OH)_x$species bound on titania catalyze the low-temperature water-gas shift reaction, J. Am. Chem. Soc. 135 (2013) 3768–3771.
[5] M. Yang, S. Li, Y. Wang, J.A. Herron, Y. Xu, M. Mavrikakis, L.F. Allard, S. Lee, J. Huang, M. Flytzani-Stephanopoulos, Catalytically active Au-$O(OH)_x$- species stabilized by alkali ions on zeolites and mesoporous oxides, Science 346 (2014) 1498–1501.
[6] M. Yang, J. Liu, S. Lee, B. Zugic, J. Huang, L.F. Allard, M. Flytzani-Stephanopoulos, A common single-site Pt(II)–$O(OH)_x$– species stabilized by sodium on "active" and "inert" supports catalyzes the water-gas shift reaction, J. Am. Chem. Soc. 137 (2015) 3470–3473.
[7] J.D. Kistler, N. Chotigkrai, P. Xu, B. Enderle, P. Praserthdam, C.Y. Chen, N.D. Browning, B.C. Gates, A single-site platinum CO oxidation catalyst in zeolite KLTL: microscopic and spectroscopic determination of the locations of the platinum atoms, Angew. Chem., Int. Ed. 53 (2014) 8904–8907.
[8] B. Qiao, A. Wang, X. Yang, L.F. Allard, Z. Jiang, Y. Cui, J. Liu, J. Li, T. Zhang, Single-atom Catalysis of CO Oxidation Using Pt_1/FeO_x, Nat. Chem. 3 (2011) 634–641.
[9] E.J. Peterson, A.T. DeLaRiva, S. Lin, R.S. Johnson, H. Guo, J.T. Miller, J.H. Kwak, C.H.F. Peden, B. Kiefer, L.F. Allard, F.H. Ribeiro, A.K. Datye, Low-Temperature carbon monoxide oxidation catalysed by regenerable atomically dispersed palladium on alumina, Nat. Commun. 5 (2014) 4885.
[10] C.K. Narula, L.F. Allard, G.M. Stocks, M. Moses-DeBusk, Remarkable NO oxidation on single supported platinum atoms, Sci. Rep. 4 (2014) 7238.
[11] Q. Fu, H. Saltsburg, M. Flytzani-Stephanopoulos, Active nonmetallic Au and Pt species on ceria-based water-gas shift catalysts, Science 301 (2003) 935–938.

[12] Y. Nagai, K. Dohmae, Y. Ikeda, N. Takagi, T. Tanabe, N. Hara, G. Guilera, S. Pascarelli, M.A. Newton, O. Kuno, H. Jiang, H. Shinjoh, S. Matsumoto, In situ redispersion of platinum autoexhaust catalysts: an on-line approach to increasing catalyst lifetimes? Angew. Chem. Int. Ed. 47 (2008) 9303–9306.

[13] J. Jones, H. Xiong, A.T. DeLaRiva, E.J. Peterson, H. Pham, S.R. Challa, G. Qi, S. Oh, M.H. Wiebenga, X.I.P. Hernández, Y. Wang, A.K. Datye, Thermally stable single-atom platinum-on-ceria catalysts via atom trapping, Science 353 (2016) 150–154.

[14] C. Bozo, N. Guilhaume, J.-M. Herrmann, Role of the ceria-zirconia support in the reactivity of platinum and palladium catalysts for methane total oxidation under lean conditions, J. Catal. 203 (2001) 393–406.

[15] M. Shen, M. Yang, J. Wang, J. Wen, M. Zhao, W. Wang, Pd/support interface-promoted $Pd-Ce_{0.7}Zr_{0.3}O_2-Al_2O_3$ automobile three-way catalysts: studying the dynamic oxygen storage capacity and CO, C_3H_8, and NO conversion, J. Phys. Chem. C 113 (2009) 3212–3221.

[16] K. Ding, A. Gulec, A.M. Johnson, N.M. Schweitzer, G.D. Stucky, L.D. Marks, Identification of active sites in CO oxidation and water-gas shift over supported Pt catalysts, Science 350 (2015) 189–192.

[17] Z. Zhang, Y. Zhu, H. Asakura, B. Zhang, J. Zhang, M. Zhou, Y. Han, T. Tanaka, A. Wang, T. Zhang, N. Yan, Thermally stable single atom $Pt/m-Al_2O_3$ for selective hydrogenation and CO oxidation, Nat. Commun. 8 (2017) 16100.

[18] J. Yang, V. Tschamber, D. Habermacher, F. Garin, P. Gilot, Effect of sintering on the catalytic activity of a Pt based catalyst for CO oxidation: experiments and modeling, Appl. Catal. B 83 (2008) 229–239.

[19] S.B. Simonsen, I. Chorkendorff, S. Dahl, M. Skoglundh, K. Meinander, T.N. Jensen, J.V. Lauritsen, S. Helveg, Effect of particle morphology on the ripening of supported Pt nanoparticles, J. Phys. Chem. C 116 (2012) 5646–5653.

[20] D. Chan, S. Tischer, J. Heck, C. Diehm, O. Deutschmann, Correlation between catalytic activity and catalytic surface area of A Pt/Al_2O_3DOC: an experimental and microkinetic modeling study, Appl. Catal. B 156 (2014) 153–165.

[21] J.H. Kwak, J. Hu, A. Lukaski, D.H. Kim, J. Szanyi, C.H.F. Peden, Role of penta-coordinated Al^{3+} ions in the high temperature phase transformation of γ-Al_2O_3, J. Phys. Chem. C 112 (2008) 9486–9492.

[22] S. Wang, A.Y. Borisevich, S.N. Rashkeev, M.V. Glazoff, K. Sohlberg, S.J. Pennycook, S.T. Pantelides, Dopants adsorbed as single atoms prevent degradation of catalysts, Nat. Mater. 3 (2004) 274–274.

[23] T. Montini, R. Singh, P. Das, B. Lorenzut, N. Bertero, P. Riello, A. Benedetti, G. Giambastiani, C. Bianchini, S. Zinoviev, S. Miertus, P. Fornasiero, Renewable H_2 from glycerol steam reforming: effect of La_2O_3 and CeO_2 addition to Pt/Al_2O_3 catalysts, ChemSusChem 3 (2010) 619–628.

[24] J.C.S. Araújo, A.L.G. Pinheiro, A.C. Oliveira, M.G.A. Cruz, J.M.C. Bueno, R.S. Araujo, R. Lang, Catalytic assessment of nanostructured Pt/La_2O_3-Al_2O_3oxides for hydrogen production by dry reforming of methane: effect of the lanthana content on the catalytic activity, Catal. Today (2018), https://doi.org/10.1016/j.cattod.2018.04.066.

[25] H. An, P.J. McGinn, Catalytic behavior of potassium containing compounds for diesel soot combustion, Appl. Catal. B 62 (2006) 46–56.

[26] R.G. Pearson, Hard and Soft acids and bases, J. Am. Chem. Soc. 85 (1963) 3533–3539.

[27] R.G. Pearson, Acids and bases, Science 14 (1966) 172–177.

[28] M. Piacentini, M. Maciejewski, A. Baiker, Pt-Ba/alumina NO_x storage-reduction catalysts: influence of Ba loading on NO_x storage behavior, Appl. Catal. B 60 (2005) 265–275.

[29] L. Castoldi, R. Matarrese, L. Lietti, P. Forzatti, Simultaneous removal of NO_x and soot on Pt–Ba/Al_2O_3 NSR catalysts, Appl. Catal. B 64 (2006) 25–34.

[30] R.D. Clayton, M.P. Harold, V. Balakotaiah, C.Z. Wan, Pt dispersion effects during NO_x storage and reduction on $Pt/BaO/Al_2O_3$ catalysts, Appl. Catal. B 90 (2009) 662–676.

[31] J.G. McCarty, K.H. Lau, D.L. Hildenbrand, Catalyst Deactivation (Elsevier Science B. V, (1997), pp. 601–607.

[32] P.N. Plessow, F. Abild-Pedersen, Sintering of Pt nanoparticles via volatile PtO_2: simulation and comparison with experiments, ACS Catal. 6 (2016) 7098–7108.

[33] J.S. Church, N.W. Cant, Surface area stability and characterization of a novel sulfate-based alumina modified by rare earth and alkaline earth ions, Appl. Catal. A Gen. 107 (1994) 267–276.

[34] Z. Liu, J.A. Anderson, Influence of reductant on the thermal stability of stored NO_x in $Pt/Ba/Al_2O_3$ NO_x storage and reduction traps, J. Catal. 224 (2004) 18–27.

[35] Z. Vít, D. Gulková, L. Kaluža, S. Bakardieva, M. Boaro, Mesoporous silica–alumina modified by acid leaching as support of Pt catalysts in HDS of model compounds, Appl. Catal. B 100 (2010) 463–471.

[36] C.H. Kim, G. Qi, K. Dahlberg, W. Li, Strontium-doped perovskites rival platinum catalysts for treating NO_x in simulated diesel exhaust, Science 327 (2010) 1624–1627.

[37] Y. Lou, J. Liu, CO oxidation on metal oxide supported single Pt atoms: the role of the support, Ind. Eng. Chem. Res. 56 (2017) 6916–6925.

[38] A.D. Allian, K. Takanabe, K.L. Fujdala, X. Hao, T.J. Truex, J. Cai, C. Buda, M. Neurock, E. Iglesia, Chemisorption of CO and mechanism of CO oxidation on supported platinum nanoclusters, J. Am. Chem. Soc. 133 (2011) 4498–4517.

[39] S.J. Schmieg, D.N. Belton, Effect of hydrothermal aging on oxygen storage/release and activity in a commercial automotive catalyst, Appl. Catal. B 6 (1995) 127–144.

[40] H. Oh, I.S. Pieta, J. Luo, W.S. Epling, Reaction kinetics of C_3H_6 oxidation for various reaction pathways over diesel oxidation catalysts, Top. Catal. 56 (2013) 1916–1921.

[41] U. Oran, D. Uner, Mechanisms of CO oxidation reaction and effect of chlorine ions on the CO oxidation reaction over Pt/CeO_2 and $Pt/CeO_2/\gamma$-Al_2O_3 catalysts, Appl. Catal. B 54 (2004) 183–191.

[42] P. Bazin, O. Saur, J.C. Lavalley, M. Daturi, G. Blanchard, FT-IR study of CO adsorption on Pt/CeO_2: characterisation and structural rearrangement of small Pt particles, Phys. Chem. Chem. Phys. 7 (2005) 187–194.

[43] G. Busca, E. Finocchio, V.S. Escribano, Infrared studies of CO Oxidation by oxygen and by water over $Pt/Al_2O_3$and Pd/Al_2O_3 catalysts, Appl. Catal. B 113 (2012) 172–179.

[44] J.R. Gaudet, A. de la Riva, E.J. Peterson, T. Bolin, A.K. Datye, Improved low-temperature CO oxidation performance of Pd supported on La-stabilized alumina, ACS Catal. 3 (2013) 846–855.

[45] H. Muraki, S.I. Matunaga, H. Shinjoh, M.S. Wainwright, D.L. Trimm, The effect of steam and hydrogen in promoting the oxidation of carbon monoxide over a platinum on alumina catalyst, J. Chem. Tech. Biotechnol. 52 (1991) 415–424.

[46] R.H. Nibbelke, M.A.J. Campman, J.H.B.J. Hoebink, G.B. Marin, Kinetic study of the CO oxidation over Pt/γ-Al_2O_3 and $Pt/Rh/CeO_2/\gamma$-Al_2O_3 in the presence of H_2O and CO_2, J. Catal. 171 (1997) 358–373.

[47] I. Lefort, J.M. Herreros, A. Tsolakis, Reduction of low temperature engine pollutants by understanding the exhaust species interactions in a diesel oxidation catalyst, Environ. Sci. Technol. 48 (2014) 2361–2367.

[48] A.B. Arvajová, J. Březina, R. Pečinka, P. Kočí, Modeling of two-step CO oxidation light-off on Pt/γ-Al_2O_3 in the presence of C_3H_6 and NO_x, Appl. Catal. B 233 (2018) 167–174.

[49] J.H. Kwak, D. Mei, C.W. Yi, D.H. Kim, C.H.F. Peden, L.F. Allard, J. Szanyi, Understanding the nature of surface nitrates in BaO/γ-Al_2O_3 NO_x storage materials: A combined experimental and theoretical study, J. Catal. 261 (2009) 17–22.

[50] Y. Nishio, M. Ozawa, Formation of featured nano-structure in thermal stable La-doped alumina composite catalyst, J. Alloys. Compd. 488 (2009) 546–549.

[51] A. Borodzinski, M. Bonarowska, Relation between crystallite size and dispersion on supported metal catalysts, Langmuir 13 (1997) 5613–5620.

[52] L. DeRita, S. Dai, K. Lopez-Zepeda, N. Pham, G.W. Graham, X. Pan, P. Christopher, Catalyst architecture for stable single atom dispersion enables site-specific spectroscopic and reactivity measurements of CO adsorbed to Pt atoms, oxidized Pt clusters, and metallic Pt clusters on TiO_2, J. Am. Chem. Soc. 139 (2017) 14150–14165.

[53] A.S. Hoffman, L.M. Debefve, S. Zhang, J.E. Perez-Aguilar, E.T. Conley, K.R. Justl, I. Arslan, D.A. Dixon, B.C. Gates, beating heterogeneity of single-site catalysts: MgO-supported iridium complexes, ACS Catal. 8 (2018) 3489–3498.

[54] L. Nie, D. Mei, H. Xiong, B. Peng, Z. Ren, X.I.P. Hernandez, A. DeLaRiva, M. Wang, M.H. Engelhard, L. Kovarik, A.K. Datye, Y. Wang, Activation of surface lattice oxygen in single-atom Pt/CeO_2 for low-temperature CO oxidation, Science 358 (2017) 1419–1423.

[55] J.T. Miller, A.J. Kropf, Y. Zha, J.R. Regalbuto, L. Delannoy, C. Louis, E. Bus, J.A. van Bokhoven, The effect of gold particle size on Au-Au bond length and reactivity toward oxygen in supported catalysts, J. Catal. 240 (2006) 222–234.

[56] J. Ke, W. Zhu, Y. Jiang, R. Si, Y.-J. Wang, S.-C. Li, C. Jin, H. Liu, W.-G. Song, C.-H. Yan, Y.-W. Zhang, strong local coordination structure effects on subnanometer PtO_x clusters over CeO_2 nanowires probed by low-temperature CO oxidation, ACS Catal. 5 (2015) 5164–5173.

[57] M. Moses-DeBusk, M. Yoon, L.F. Allard, D.R. Mullins, Z. Wu, X.F. Yang, G. Veith, G.M. Stocks, C.K. Narula, CO oxidation on supported single Pt atoms: experimental and ab initio density functional studies of CO interaction with Pt atom on θ-Al_2O_3(010) surface, J. Am. Chem. Soc. 135 (2013) 12634–12645.

[58] NIST X-ray Photoelectron Spectroscopy Database. https://srdata.nist.gov/xps/default.aspx (Accessed December 2016).

[59] A. Boubnov, S. Dahl, E. Johnson, A.P. Molina, S.B. Simonsen, F.M. Cano, S. Helveg, L.J. Lemus-Yegres, J.D. Grunwaldt, Structure–activity relationships of Pt/Al_2O_3 catalysts for CO and NO oxidation at diesel exhaust conditions, Appl. Catal. B 126 (2012) 315–325.

[60] T.K. Hansen, M. Høj, B.B. Hansen, T.V.W. Janssens, A.D. Jensen, The effect of Pt particle size on the oxidation of CO, C_3H_6, and NO Over $Pt/Al_2O_3$for diesel exhaust after treatment, Top. Catal. 60 (2017) 1333–1344.

[61] M. Cargnello, V. Doan-Nguyen, T.R. Gordon, R.E. Diaz, E.A. Stach, R.J. Gorte, P. Fornasiero, C.B. Murray, Control of metal nanocrystal size reveals metal-support interface role for Ceria catalysts, Science 341 (2013) 771–773.

[62] M. Shekhar, J. Wang, W.S. Lee, W.D. Williams, S.M. Kim, E.A. Stach, J.T. Miller, W.N. Delgass, F.H. Ribeiro, Size and support effects for the water-gas shift catalysis over gold nanoparticles supported on model Al_2O_3 and TiO_2, J. Am. Chem. Soc. 134 (2012) 4700–4708.

[63] T. Fujitani, I. Nakamura, Mechanism and active sites of the oxidation of CO over Au/TiO_2, Angew. Chem. Int. Ed. 50 (2011) 10144–10147.

[64] D. Widmann, R.J. Behm, Active oxygen on A Au/TiO_2 catalyst: formation, stability, and CO oxidation activity, Angew. Chem. Int. Ed. 50 (2011) 10241–10245.

[65] R.K. Herz, S.P. Marin, Surface chemistry models of carbon monoxide oxidation on supported platinum catalysts, J. Catal. 65 (1980) 281–296.

[66] M.J. Kale, P. Christopher, Utilizing quantitative in situ FTIR spectroscopy to identify well-coordinated Pt atoms as the active site for CO oxidation on Al_2O_3-supported Pt catalysts, ACS Catal. 6 (2016) 5599–5609.